

Mass splitting and spin alignment for ϕ mesons in a magnetic field in NJL model

Xin-Li Sheng,^{1,*} Shu-Yun Yang,¹ Yao-Lin Zou,¹ and Defu Hou^{1,†}

¹*Key Laboratory of Quark and Lepton Physics (MOE) and Institute of Particle Physics,
Central China Normal University, Wuhan, 430079, China*

Based on the Nambu-Jona-Lasinio (NJL) model, we develop a framework for calculating the spin alignment of vector mesons and applied it to study ϕ mesons in a magnetic field. We calculate mass spectra for ϕ mesons and observe mass splitting between the longitudinally polarized state and the transversely polarized state. The ϕ meson in a thermal equilibrium system is preferred to occupy the state with spin $\lambda = 0$ than those with spin $\lambda = \pm 1$, because the former state has smaller energy. As a consequence, we conclude that the spin alignment will be larger than $1/3$ if one measures along the direction of the magnetic field, which is qualitatively consistent with the recent STAR data. Around the critical temperature $T_C = 150$ MeV, the positive deviation from $1/3$ is proportional to the square of the magnetic field strength, which agrees with the result from the non-relativistic coalescence model. Including the anomalous magnetic moments for quarks will modify the dynamical masses of quarks and thus influence the mass spectra and spin alignment of ϕ mesons. The discussion of spin alignment in the NJL model may help us better understand the formation of hadron's spin structure during the chiral phase transition.

I. INTRODUCTION

Non-central relativistic heavy-ion collisions provide a unique opportunity to study quantum chromodynamics (QCD) matter in a strong magnetic field [1]. The hot and dense matter created in collisions is known as the quark-gluon plasma (QGP), which evolves with time and cools down to the hadronic phase at the freeze-out time. In Au-Au collisions at the Relativistic Heavy Ion Collider (RHIC) or Pb-Pb collisions at the Large Hadron Collider (LHC), the magnetic field perpendicular to the reaction plane can reach $5m_\pi^2 \sim 10^{18}$ Gauss (m_π is the pion mass) or even larger [2–6]. Such a strong magnetic field is mainly generated by spectators in the colliding nuclei. It drops fastly with time, but the existence of medium electrical conductivity will extend its lifetime [7–13]. Therefore it may have sizeable contributions to many phenomena, for example, the chiral magnetic effect [2, 14, 15], the Λ 's polarization [16–18], and the charge-odd directed flow [8, 19–22]. On the other hand, the electromagnetic fields also have event-by-event fluctuations, which are still significantly large even in the late stage of collisions [5, 23, 24]. The fluctuating fields thus contribute to phenomena at the freeze-out time, such as the magnetic catalysis [25–29], the inverse magnetic catalysis [29, 30], and the phase structure of the QGP [26, 31–33].

Recently, the STAR collaboration has measured the ϕ and K^{*0} meson's spin alignment along the out-of-plane direction and observes a significant positive deviation from $1/3$ for the ϕ meson [34]. The spin alignment refers to the 00-element of the normalized spin density matrix for a vector meson with spin-1 [35, 36]. The positive derivation from $1/3$ observed in experiments indicates that the spin of ϕ meson is preferred to align in the reaction plane. According to the quark coalescence model,

the spin alignment of vector meson is induced by polarizations of its constitute quarks [35, 37] and thus have various sources such as the vorticity fields [35, 37, 38], the electromagnetic fields [37], the helicity polarization [39], the turbulent color fields [40], the shear stress [41, 42], and the strong force field [43–46]. Among these works, only the fluctuations of the strong force field successfully reproduce the experiment data [46]. Since the strong force field in [46] has the same structure as the classical electromagnetic field, one naturally expects that fluctuations of electromagnetic fields, rather than their event-average values, also contribute to the spin alignment of vector mesons.

In this work, we study the spin alignment of ϕ meson in a constant magnetic field using the three flavor Nambu-Jona-Lasinio (NJL) model [47–54]. Such a field configuration can be straightforwardly extended to the case of a space-time dependent magnetic field with the typical length of its inhomogeneity much larger than the typical hadron size. In the NJL model, gluons are integrated out and quarks interact via local four-fermion interactions, which have the form that keeps the chiral symmetry. Mesons are treated as quantum fluctuations beyond a constant mean-field and their propagators are introduced through the random phase approximation by the resummation of quark bubbles [51, 52, 55]. The mass spectra for mesons are given by the poles, or equivalently, by the imaginary part of their propagators. Within the framework of magnetized NJL model, the spectra of light-flavor mesons, including σ , π^0 , π^\pm , ω , ρ^0 , and ρ^\pm , have attracted a lot of interest [56–64], but few works focus on the ϕ meson. One can refer to [33, 65, 66] for recent reviews on the NJL model in a strong magnetic field. In this manuscript, we observe the splitting between masses of ϕ mesons in different spin states, which is induced by the magnetization of the constitute quark and antiquark. In a hot and thermal equilibrium system, the mass splitting leads to different spin-dependent equilibrium distributions and thus corresponds to a non-

* xls@mail.ccnu.edu.cn

† houdf@mail.ccnu.edu.cn

trivial spin alignment. We also study the effect of quark anomalous magnetic moments (AMM) considering that constitute quarks have different magnetic moments compared with free quarks [61, 62, 67–70]. The AMMs are included in the fermion Hamiltonian by putting a new term $q_f \kappa_f F_{\mu\nu} \sigma^{\mu\nu} / 2$, where $F^{\mu\nu}$ is the electromagnetic field tensor, $\sigma^{\mu\nu} \equiv (i/2)[\gamma^\mu, \gamma^\nu]$, and q_f, κ_f are the charge and the AMM for a quark with flavor $f = u, d, s$. The AMMs change the dynamical masses of quarks and therefore affect the spectra and spin alignment of the ϕ meson.

This manuscript is organized as follows. In Sec. II we review the theoretical framework for the three flavor NJL model. Then in Sec. III we give analytical formulas for vector meson's propagator, spectral function, and spin alignment. We numerically calculated the quark mass, ϕ meson's spectra and spin alignment. All the numerical results are given in Sec. IV. Finally, in Sec. V we summarize our findings and conclude.

II. NAMBU-JONA-LASINIO MODEL

In order to describe a strongly-interaction quark matter, we use the three-flavor Nambu-Jona-Lasinio model with scalar and vector channels of four-fermion interactions [51–53, 55],

$$\begin{aligned} \mathcal{L}_{\text{eff}} = & \mathcal{L}_q + G_S \sum_{a=0}^8 [(\bar{\psi} \lambda_a \psi)^2 + (\bar{\psi} i \gamma_5 \lambda_a \psi)^2] \\ & - G_V \sum_{a=0}^8 [(\bar{\psi} \gamma_\mu \lambda_a \psi)^2 + (\bar{\psi} i \gamma_\mu \gamma_5 \lambda_a \psi)^2] \\ & - K \{ \det_f [\bar{\psi} (1 + \gamma_5) \psi] + \det_f [\bar{\psi} (1 - \gamma_5) \psi] \}, \end{aligned} \quad (1)$$

where $\psi = (\psi_u, \psi_d, \psi_s)$ are Dirac spinors for u, d , and s quarks, respectively, λ_a with $a = 1, 2, \dots, 8$ are Gell-Mann matrices, and $\lambda_0 = \sqrt{2/3} I_0$ with I_0 being the identity matrix in the color space. The last term is the six-quark Kobayashi-Maskawa - 't Hooft interaction that breaks the $U_A(1)$ symmetry [71]. Here G_S and G_V are coupling constants for scalar and vector interactions, respectively. The Lagrangian \mathcal{L}_q for quarks in an external electromagnetic field $F^{\mu\nu}$ is given by

$$\mathcal{L}_q = \sum_{f=u,d,s} \bar{\psi}_f \left(i \gamma_\mu D_f^\mu - m_f - \frac{1}{2} q_f \kappa_f F_{\mu\nu} \sigma^{\mu\nu} \right) \psi_f, \quad (2)$$

where m_f and κ_f denote current quark masses and AMMs, respectively, for quarks with flavor $f = u, d, s$. The covariant derivative $D_f^\mu \equiv \partial^\mu + i q_f A^\mu$ with q_f being the quark charges and A^μ being the gauge potential for the external electromagnetic field. Here we include AMMs κ_f in order to reproduce the phenomenological constitute quark magnetic moments in the zero-temperature limit. Under the mean-field approximation,

the Lagrangian becomes

$$\begin{aligned} \mathcal{L}_{\text{MF}} = & \sum_{f=u,d,s} \bar{\psi}_f \left[i \gamma_\mu D_f^\mu - M_f + i q_f \kappa_f B \gamma^1 \gamma^2 \right] \psi_f \\ & - 2G_S \sum_{f=u,d,s} \sigma_f^2 + 4K \sigma_u \sigma_d \sigma_s, \end{aligned} \quad (3)$$

where σ_f is the quark chiral condensate $\sigma_f \equiv \langle \bar{\psi}_f \psi_f \rangle$. The dynamical mass M_f is defined as

$$M_f \equiv m_f - 4G_S \sigma_f + 2K \prod_{f' \neq f} \sigma_{f'}, \quad (4)$$

where the last term arises from the 't Hooft interaction.

We consider a magnetic field along the z -direction and take the Landau gauge $A^\mu = (0, 0, Bx, 0)$ with the magnetic field strength $B > 0$ without loss of generality. For each flavor of quark, it is straightforward to derive the Dirac equation from the Lagrangian (3),

$$\left(i \gamma_\mu D_f^\mu - M_f + i q_f \kappa_f B \gamma^1 \gamma^2 \right) \psi_f = 0. \quad (5)$$

Assuming that the magnetic field is a constant number and the considered system is homogeneous, the Dirac equation can be analytically solved by applying the Ritus method [72, 73]. The resulting dispersion relation for the n -th Landau level reads,

$$\begin{aligned} E = & \pm E_{f,n,s}(p_z) \\ = & \pm \sqrt{p_z^2 + \left(\sqrt{M_f^2 + 2n|q_f B|} - s \kappa_f |q_f B| \right)^2}, \end{aligned} \quad (6)$$

where the momentum perpendicular to the z -direction is quantized as the Landau levels, while the longitudinal momentum is not restricted. Here $s = +$ for the lowest Landau level and $s = \pm$ for Landau levels $n \geq 1$ denote the spin state. The positive and negative energies are related to particles and antiparticles, respectively. Using Eq. (6), the quark grand thermodynamic potential Ω_f can be written as

$$\begin{aligned} \Omega_f = & \frac{N_c |q_f B|}{4\pi^2} \sum_{n,s} \int dp_z \left\{ \frac{E_{f,n,s}(p_z)}{2} \right. \\ & \left. + 2T \ln \left[1 + e^{-E_{f,n,s}(p_z)/T} \right] \right\}, \end{aligned} \quad (7)$$

where T is the temperature and $N_c = 3$ is the degeneracy of color. The summation in Eq. (7) runs over $s = +$ for $n = 0$ and $s = \pm$ for $n = 1, 2, 3, \dots$. The total grand potential for the whole quark-meson system includes Ω_f and the mean field part, which is given by

$$\Omega = \sum_{f=u,d,s} (2G_S \sigma_f^2 - \Omega_f) + 4K \sigma_u \sigma_d \sigma_s. \quad (8)$$

The quark condensates σ_f and the corresponding quark masses M_f are then calculated by minimizing the grand potential, $\partial \Omega / \partial \sigma_f = 0$.

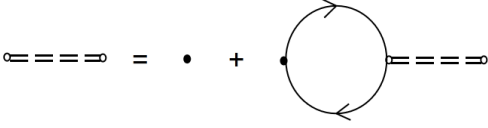


Figure 1. Dyson-Schwinger equation for vector meson's propagator. Solid lines denote quark propagators and dashed lines denote meson propagator. Four-quark vertices with black dots correspond to the vector-type four-fermion interaction.

Following Ref. [65], the free quark propagator in momentum space is expressed as follows with the help of the eigenenergies in Eq. (6),

$$S_f(p) = \sum_{n=0}^{\infty} \frac{i\tilde{S}_{f,n}(p)}{\prod_{s=\pm} \left\{ (p^0)^2 - [E_{f,n,s}(p_z)]^2 + i\epsilon \right\}}, \quad (9)$$

where the numerator is given by

$$\tilde{S}_f(p) = e^{-p_{\perp}^2/|q_f B|} (-1)^n D_n^f(p) \frac{U_n}{\mathcal{M}(p) - 2n|q_f B|}, \quad (10)$$

with explicit expressions of $D_n^f(p)$, U_n and $1/[\mathcal{M}(p) - 2n|q_f B|]$ are given in Ref. [65] and also in Appendix A. The poles in Eq. (9) are shifted above or below the real axis by an infinite small imaginary part $\pm i\epsilon$ such that $S_f(p)$ denotes the Feynmann propagator.

III. PROPAGATOR AND SPIN ALIGNMENT OF VECTOR MESONS

In the NJL model, the propagator of a vector meson is obtained by taking the quark bubble summation in the random phase approximation. This leads to the Dyson-Schwinger equation shown in Fig. 1,

$$D^{\mu\nu}(k) = 4G_V \Delta^{\mu\nu}(k) + 4G_V \Delta^{\mu\alpha}(k) \Sigma_{\alpha\beta}(k) D^{\beta\nu}(k), \quad (11)$$

where $D^{\mu\nu}$ is the vector meson's propagator and $\Sigma^{\mu\nu}$ is the self-energy at the one-loop level. The projection operator $\Delta^{\mu\nu}(k) \equiv g^{\mu\nu} - k^{\mu}k^{\nu}/k^2$ ensures $k_{\mu}D^{\mu\nu}(k) = 0$. Using the quark propagator in Eq. (9), the self-energy is given by

$$\Sigma^{\mu\nu}(k) = -iN_c \int \frac{d^4p}{(2\pi)^4} \text{Tr} [\gamma^{\mu} S_f(k+p) \gamma^{\nu} S_{f'}(p)], \quad (12)$$

where the quark flavors f and f' depend on the type of considered meson. In this work we focus the ϕ meson and thus we take $f = f' = s$ in Eq. (12).

As spin-1 particles, the vector mesons have three spin states $\lambda = 0, \pm 1$. If we choose the spin quantization direction as the z -direction in the meson's rest frame, we

have the following spin polarization vectors,

$$\begin{aligned} \epsilon_0 &= (0, 0, 1), \\ \epsilon_{+1} &= -\frac{1}{\sqrt{2}}(1, i, 0), \\ \epsilon_{-1} &= \frac{1}{\sqrt{2}}(1, -i, 0), \end{aligned} \quad (13)$$

corresponding to $\lambda = 0, \pm 1$, respectively. In general, if the spin quantization direction is taken as the direction of an unit vector \mathbf{n} , we have $\epsilon_0 = \mathbf{n}$ and $\epsilon_{\pm 1}$ are perpendicular to \mathbf{n} . By taking a Lorentz boost, we derive the covariant form of spin polarization vectors,

$$\epsilon^{\mu}(\lambda, k) = \left(\frac{\mathbf{k} \cdot \epsilon_{\lambda}}{m_V}, \epsilon_{\lambda} + \frac{\mathbf{k} \cdot \epsilon_{\lambda}}{m_V(\omega + m_V)} \mathbf{k} \right), \quad (14)$$

where $k^{\mu} \equiv (\omega, \mathbf{k})$ is the four-momentum and $m_V = \sqrt{\omega^2 - \mathbf{k}^2}$ is the mass of the vector meson. These vectors are perpendicular to k^{μ} , $k_{\mu}\epsilon^{\mu}(\lambda, k) = 0$, and are properly normalized as $\epsilon^{\mu*}(\lambda, k)\epsilon_{\mu}(\lambda', k) = -\delta_{\lambda\lambda'}$. Using these vectors, the meson propagator $D^{\mu\nu}(k)$ can be cast into the following form,

$$D^{\mu\nu}(k) = \sum_{\lambda, \lambda'=0, \pm 1} \epsilon^{\mu*}(\lambda, k)\epsilon^{\nu}(\lambda', k) D_{\lambda\lambda'}(k), \quad (15)$$

The element $D_{\lambda\lambda'}(k)$ is a Lorentz invariant function that is given by projecting $D^{\mu\nu}(k)$ onto $\epsilon_{\mu}(\lambda, k)\epsilon_{\nu}^*(\lambda', k)$,

$$D_{\lambda\lambda'}(k) = \epsilon_{\mu}(\lambda, k)\epsilon_{\nu}^*(\lambda', k) D^{\mu\nu}(k). \quad (16)$$

Similarly, projecting the Dyson-Schwinger equation in (11) onto $\epsilon_{\mu}(\lambda, k)\epsilon_{\nu}^*(\lambda', k)$ gives the equation for $D_{\lambda\lambda'}(k)$,

$$D_{\lambda\lambda'}(k) = -4G_V \delta_{\lambda\lambda'} - 4G_V \sum_{\lambda_1=0, \pm 1} \Sigma_{\lambda\lambda_1}(k) D_{\lambda_1\lambda'}(k), \quad (17)$$

which have solution of the following form,

$$D_{\lambda\lambda'}(k) = - \left[\frac{4G_V}{1 + 4G_V \Sigma(k)} \right]_{\lambda\lambda'}. \quad (18)$$

Note that $\Sigma(k)$ in the denominator is a short-handed notation for the 3×3 matrix $\Sigma_{\lambda\lambda'}(k)$, which is defined as

$$\Sigma_{\lambda\lambda'}(k) = \epsilon_{\mu}(\lambda, k)\epsilon_{\nu}^*(\lambda', k) \Sigma^{\mu\nu}(k). \quad (19)$$

The density matrix for the vector meson in a thermal equilibrium system is given by the convolution of its spectral function and the Bose-Einstein distribution,

$$\bar{\rho}_{\lambda\lambda'}(\mathbf{k}) = \int d\omega \frac{2\omega}{e^{\omega/T} - 1} \xi_{\lambda\lambda'}(k), \quad (20)$$

where the spectral function is derived from the imaginary part of the full propagator [55],

$$\xi_{\lambda\lambda'}(k) \equiv \frac{1}{\pi} \text{Im} D_{\lambda\lambda'}(k). \quad (21)$$

The spin alignment is then given by the 00-element of the normalized density matrix,

$$\rho_{00}(\mathbf{k}) \equiv \frac{\bar{\rho}_{00}(\mathbf{k})}{\sum_{\lambda=0,\pm 1} \bar{\rho}_{\lambda\lambda}(\mathbf{k})}. \quad (22)$$

The result in a constant magnetic field can be evaluated by using Eqs. (9,12,18-22). When calculating the self-energy in (12), we substitute the energy integral with a summation over Matsubara frequencies at finite temperature [74]. This allows us to study the meson properties at finite temperature.

We emphasize that Eqs. (18-22) are universal formulas, which can be applied in calculating momentum-dependent spin alignments along any measuring direction. However, it will significantly simplify our calculation to focus on a rest meson $\mathbf{k} = \mathbf{0}$ and choose the measuring direction as the z -direction. The corresponding spin polarization vectors as given in Eq. (13). Due to the rotational invariance in the $x - y$ plane, one can also prove that $\Sigma_{\lambda\lambda'}$, $D_{\lambda\lambda'}$, and the density matrix $\bar{\rho}_{\lambda\lambda'}(\mathbf{0})$ are diagonal in the spin space,

$$\bar{\rho}_{\lambda\lambda'}(\mathbf{0}) = \begin{pmatrix} \bar{\rho}_{11} & 0 & 0 \\ 0 & \bar{\rho}_{00} & 0 \\ 0 & 0 & \bar{\rho}_{-1,-1} \end{pmatrix}, \quad (23)$$

where the states with $\lambda = \pm 1$ are degenerate, $\bar{\rho}_{-1,-1} = \bar{\rho}_{11}$. In general, if the measuring direction is characterized by Euler angles (α, β, γ) , the density matrix is calculated by performing a rotation in spin space,

$$\bar{\rho}_{\lambda\lambda'}(\mathbf{0}; \alpha, \beta, \gamma) = \sum_{\lambda_1, \lambda_2} R_{\lambda\lambda_1}(\alpha, \beta, \gamma) \bar{\rho}_{\lambda_1\lambda_2}(\mathbf{0}) R_{\lambda_2\lambda'}^{-1}(\alpha, \beta, \gamma), \quad (24)$$

where $R_{\lambda\lambda'}(\alpha, \beta, \gamma)$ is the spin-1 representation of the rotation with Euler angles (α, β, γ) . Here $\bar{\rho}_{\lambda_1\lambda_2}(\mathbf{0})$ is the density matrix when measuring along the z -direction. A straightforward calculation shows that the spin alignment is independent to Euler angles α and γ ,

$$\rho_{00}(\mathbf{0}; \alpha, \beta, \gamma) = \frac{\bar{\rho}_{00}(\mathbf{0}) \cos^2 \beta + \bar{\rho}_{11}(\mathbf{0}) \sin^2 \beta}{\bar{\rho}_{00}(\mathbf{0}) + 2\bar{\rho}_{11}(\mathbf{0})}. \quad (25)$$

Defining the spin alignment in the magnetic field direction as

$$\rho_{00}^B(\mathbf{0}) \equiv \frac{\rho_{00}(\mathbf{0})}{\rho_{00}(\mathbf{0}) + 2\rho_{11}(\mathbf{0})}, \quad (26)$$

we derive that

$$\rho_{00}(\mathbf{0}; \alpha, \beta, \gamma) = \frac{1}{2} \{ 1 - \rho_{00}^B(\mathbf{k}) + [3\rho_{00}^B(\mathbf{k}) - 1] \cos^2 \beta \}, \quad (27)$$

which only depends on ρ_{00}^B and the angle between the direction of the magnetic field and the measuring direction. For a fluctuating magnetic field, one have to take an average over the β -angle and the field strength. If the

field does not have a preferred direction, one can prove that the average $\langle \rho_{00}(\mathbf{0}; \alpha, \beta, \gamma) \rangle = 1/3$, as expected. If the fluctuations are anisotropic in space, the average spin alignment will deviate from 1/3, as predicted in Refs. [43–46].

IV. NUMERICAL RESULTS

A. Parameter settings

Since the NJL model is non-renormalizable, it is necessary to include a regularization scheme for the divergent momentum integrals in Eqs. (7) and (12). Since a sharp three-momentum cutoff will lead to nonphysical oscillations in a magnetic field, we choose a Pauli-Villas regularization scheme [75]. Any function of M_f is replaced by a summation,

$$f(M_f) \rightarrow f_{\text{P.V.}}(M_f) = \sum_{j=0}^3 c_j f\left(\sqrt{M_f^2 + j\Lambda^2}\right), \quad (28)$$

with $c_0 = 1$, $c_1 = -3$, $c_2 = 3$, and $c_3 = -1$. We take the parameter set given in [76],

$$\begin{aligned} m_{u,d} &= 10.3 \text{ MeV}, m_s = 236.9 \text{ MeV}, \Lambda = 0.7812 \text{ GeV}, \\ G_S \Lambda^2 &= 4.90, \quad K \Lambda^5 = 129.8, \end{aligned} \quad (29)$$

which are obtained by fitting vacuum values for the pion decay constant and masses of pion, kaon, η' , and constituent light-quarks. This set of parameters leads to dynamical masses $M_{u,d} = 324.7 \text{ MeV}$ and $M_s = 553.9 \text{ MeV}$ in the vacuum in absence of the magnetic field. The vector coupling constant G_V is taken as

$$G_V \Lambda^2 = -4.67, \quad (30)$$

which is obtained by fitting the ϕ meson's mass $M_\phi = 1.02 \text{ GeV}$ in the vacuum.

To evaluate the effect of AMMs for quarks, we make comparisons between two sets of parameters,

$$\kappa_u^{(1)} = \kappa_d^{(1)} = \kappa_s^{(1)} = 0, \quad (31)$$

and

$$\begin{aligned} \kappa_u^{(2)} &= 0.123 \text{ GeV}^{-1}, \kappa_d^{(2)} = 0.555 \text{ GeV}^{-1}, \\ \kappa_s^{(2)} &= 0.329 \text{ GeV}^{-1}. \end{aligned} \quad (32)$$

The later set of AMMs is fixed by phenomenological values of magnetic moments for valence quarks [77], i.e., $\mu_u = 2.08\mu_N$, $\mu_d = -1.31\mu_N$, and $\mu_s = -0.77\mu_N$, where the nuclear magneton $\mu_N \equiv e/2m_p$ with $m_p = 0.938 \text{ GeV}$ being the proton mass. In later parts of this manuscript, these two sets of AMMs are denoted as $\kappa_f = 0$ and $\kappa_f \neq 0$, respectively.

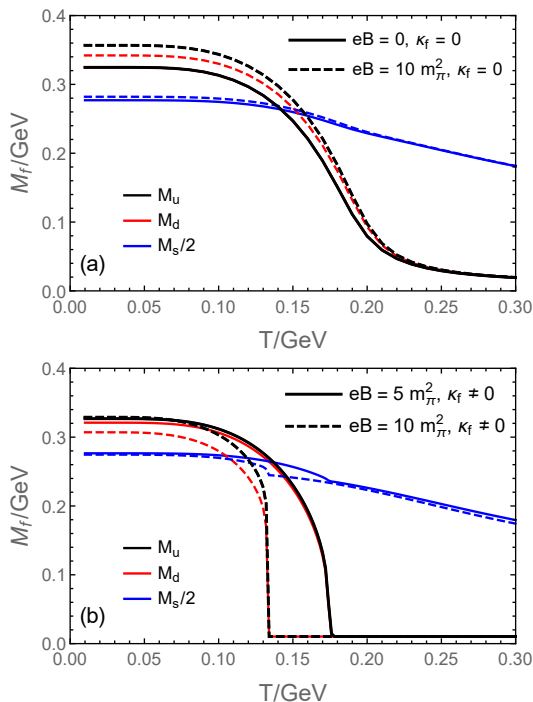


Figure 2. Dynamical masses as functions of the temperature for u quark (black lines), d quark (red lines), and s quark (blue lines). In panel (a), solid lines correspond to the case with $eB = 0$ and $\kappa_f = 0$, while dashed lines with $eB = 10 m_\pi^2$ and $\kappa_f = 0$. The panel (b) plot dynamical masses for quarks with AMMs $\kappa_f \neq 0$ in magnetic fields $eB = 5 m_\pi^2$ (solid lines) and $eB = 10 m_\pi^2$ (dashed lines).

B. Dynamic masses for quarks

We first focus on the dynamical masses for quarks, which are related to the chiral condensates σ_f as given in (4). The condensates σ_f are order parameters for the chiral phase transition. In the chiral symmetry breaking phase, $\sigma_f \neq 0$ and thus quarks have nonvanishing dynamical masses. In the chiral symmetry restored phase, $\sigma_f = 0$ and quark dynamical masses reduce to their current masses.

The behavior of dynamical masses for u , d , and s quarks as functions of the temperature is shown in Fig. 2. In Fig. 2 (a), we set AMMs $\kappa_u = \kappa_d = \kappa_s = 0$ and choose two sets of values for the magnetic field strength: solid lines for $eB = 0$ and dashed lines for $eB = 10 m_\pi^2$. We observe that the chiral phase transition is a cross-over with critical temperature around $T_C \approx 150$ MeV. Compared to the case with $eB = 0$, a larger magnetic field, $eB = 10 m_\pi^2$, corresponds to larger quark masses and slightly higher T_C , which is the behavior of the magnetic catalysis. We also observe that the u and d quarks have identical masses when $eB = 0$, but have different masses in a nonzero magnetic field. That is because the difference in electric charges, $q_u/e = +2/3$, $q_d/e = -1/3$, leads to different magnetic energies and breaks the symmetry

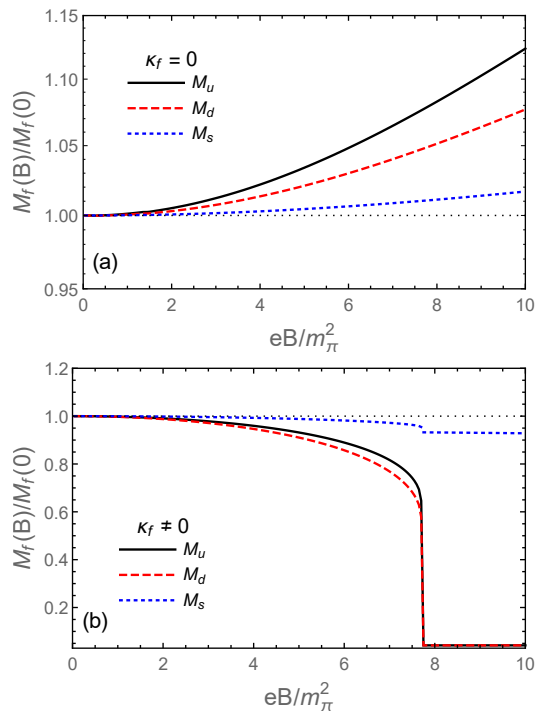


Figure 3. Dynamical masses as functions of the magnetic field strength at $T = 150$ MeV for cases with vanishing AMMs [panel (a)] and nonvanishing AMMs [panel (b)], normalized by masses when $eB = 0$. Dynamical masses for u , d , and s quarks are plotted with black solid line, red dashed line, and blue dotted line, respectively.

between light-flavor quarks. On the other hand, we show in Fig. 2 (b) the quark masses considering nonvanishing AMMs in (32), with solid and dashed lines correspond to $eB = 5 m_\pi^2$ and $eB = 10 m_\pi^2$, respectively. As T increases, masses of u and d quarks sharply decrease to their current masses, indicating a first-order phase transition that happens at 176 MeV when $eB = 5 m_\pi^2$, and at 133 MeV when $eB = 10 m_\pi^2$. On the other hand, the s quark is less affected by the AMM and still undergoes a cross-over. In the chiral symmetry breaking phase, the quark masses at $eB = 5 m_\pi^2$ is larger than those at $eB = 10 m_\pi^2$, which is the inverse magnetic catalysis phenomena.

Figure 3 focuses on the ratio of quark masses as functions of the field strength to those in absence of the magnetic field. Here we fix the temperature at the ordinary critical temperature $T = 150$ MeV. If we do not consider quark's AMMs, the quark masses grow with an increasing magnetic field, as shown in Fig. 3 (a). We find that u quark mass is more affected by the magnetic field than the d quark mass, because $|q_u| > |q_d|$. On the other hand, nonvanishing AMMs will result in the inverse magnetic catalysis, i.e., the dynamical masses decrease with an increasing magnetic field, as shown in Fig. 3 (b). Moreover, at a particular field strength, M_u and M_d suffer a discontinuity, corresponding to a first-order phase tran-

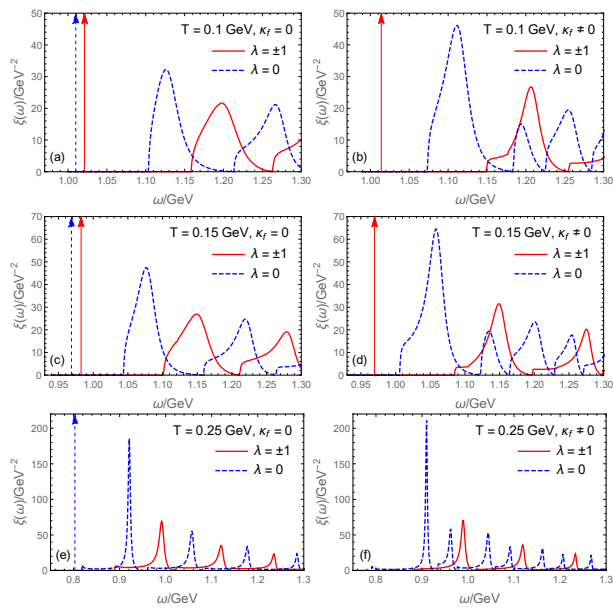


Figure 4. Mass spectra for ϕ mesons in a constant magnetic field with $eB = 5m_\pi^2$, at $T = 100$ MeV [panels (a) and (b)], $T = 150$ MeV [panels (c) and (d)], and $T = 250$ MeV [panels (e) and (f)]. The AMMs are set to zeros in panels (a), (c), and (e); and set to nonzero values given in Eq. (32) in panels (b), (d), and (f). Here red solid lines denote spectral functions for ϕ mesons with spin state $\lambda = \pm 1$ and blue dashed lines denote the spectral function of $\lambda = 0$. Red and blue arrows correspond to delta functions.

sition. For the case in Fig. 3 (b), $T = 150$ MeV, the critical field strength $eB_C = 7.75 m_\pi^2$. Above eB_C , dynamical masses for u and d quarks are consistent with the current quark masses.

C. Mass spectra for ϕ meson

Using quark masses as functions of the temperature and the magnetic field strength, we are then able to calculate the vector meson's spectral functions using Eqs. (9), (12), and (18)-(21). In this work, we focus on the vector ϕ meson, which has constitute quarks s and \bar{s} . At the one-loop level, the self-energy for the ϕ meson depends on the propagator of s quark, but does not depend on propagators of u and d quarks. We set the spin quantization direction parallel to the magnetic field and therefore the spectral function is diagonal $\xi_{\lambda\lambda'} = \text{diag}(\xi_{+1}, \xi_0, \xi_{-1})$, and spin states $\lambda = \pm 1$ are degenerate, $\xi_{+1} = \xi_{-1}$. In this work, we only focus on the mass spectra, i.e., the three-momenta of the ϕ meson are set to zeros, $\mathbf{k} = \mathbf{0}$.

In order to clearly show the influence of the magnetic field to the spectral function, we choose the magnetic field strength $eB = 5 m_\pi^2$ and plot the mass spectra for the ϕ meson at temperatures $T = 100$ MeV, 150 MeV, and 250 MeV in Fig. 4. In general, the spectral function can be separated into a delta-function part and a continuum

part as

$$\xi_\lambda(\omega, \mathbf{0}) = \delta(\omega^2 - M_{\phi,\lambda}^2) + \xi_\lambda^*(\omega). \quad (33)$$

The delta-function part is identified as a stable bound state that corresponds to a real on-shell ϕ meson with mass $M_{\phi,\lambda}$. The continuum part $\xi_\lambda^*(\omega)$ is related to unstable resonance excitations. In Fig. 4, the delta-functions are plotted as arrows. We observe a mass splitting between bound states with $\lambda = 0$ and $\lambda = \pm 1$ in Fig. 4 (a) and (c), indicating that the longitudinally polarized ϕ meson and the transversely polarized ϕ meson have different energies. The bound state masses and the thresholds for the continuum drop as T increases, which is the result of dropping quark masses. The bound states will dissociate when T is large enough, indicating a Mott transition [78–82]. In absence of AMMs, bound states with spin $\lambda = \pm 1$ dissociates at $T = 250$ MeV, c.f., Fig. 4 (e), while the bound state with $\lambda = 0$ still exist. However, if we consider nonzero AMMs, the bound state with $\lambda = 0$ vanishes for all three considered temperatures $T = 100$ MeV, 150 MeV, and 250 MeV, while states with $\lambda = \pm 1$ vanish at $T = 250$ MeV. In this work, we only consider the coupling between the ϕ meson and the s quark. In a thermal medium, the physical ϕ meson was observed to have a large broadening [83–85], which may arise from the ϕN cross-section and is beyond the scope of our discussion.

For all considered cases, the continuum part contains several well-separated peaks. One can understand the multi-peak structure of the spectral function in Fig. 4 as follows. In the presence of a magnetic field, the dispersion relation of s quark is quantized as Landau levels given in Eq. (6). Supposing the constitute s and \bar{s} quarks inside a ϕ meson are at Landau levels n_1 and n_2 , respectively, the angular momentum conservation demands that the ϕ meson with $\lambda = 0$ must be consist of quark and antiquark with $n_1 = n_2$, and the ϕ meson with $\lambda = \pm 1$ correspond to $n_1 = n_2 \pm 1$. Different sets of n_1 and n_2 give different resonance peaks as shown in Fig. 4.

We denote the energy for the most significant peak in the continuum as $M_{\phi,\lambda}^*$ and plot $M_{\phi,\lambda}$, $M_{\phi,\lambda}^*$ as functions of the temperature at $eB = 5m_\pi^2$ in Fig. 5. Similar to the temperature dependence of the s quark, the ϕ meson masses also decrease at higher temperatures. In Fig. 5 (a), the AMMs are set to zeros. One can observe the mass splitting between states with $\lambda = 0$ and $\lambda = \pm 1$: states with $\lambda = 0$ always have smaller masses compared to states with $\lambda = \pm 1$. As the temperature increases, the bound states finally dissociate, and the corresponding dissociation temperature is 215 MeV for $\lambda = \pm 1$ and 270 MeV for $\lambda = 0$. Therefore when the temperature $215 \text{ MeV} < T < 270 \text{ MeV}$, ϕ meson bound states are purely at states with $\lambda = 0$. On the other hand, if the AMMs are nonzero, as shown in Fig. 5 (b), the bound state with $\lambda = 0$ does not exist even at lower temperatures. The dissociation temperature for $\lambda = \pm 1$ states is nearly independent to the AMMs.

In Fig. 6, we show the field strength dependence for the

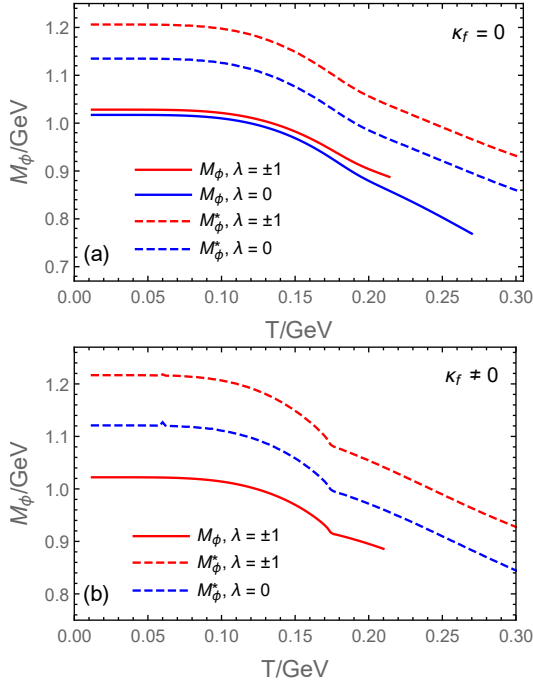


Figure 5. Dynamical masses as functions of the temperature for ϕ mesons at $eB = 5m_\pi^2$. Masses for bound states with spin $\lambda = 0$ and $\lambda = \pm 1$ are plotted with red solid lines and blue solid lines, respectively, while those for resonance excitations are plotted with red dashed lines and blue dashed lines, respectively. We take vanishing AMMs in panel (a) and nonzero AMMs in panel (b).

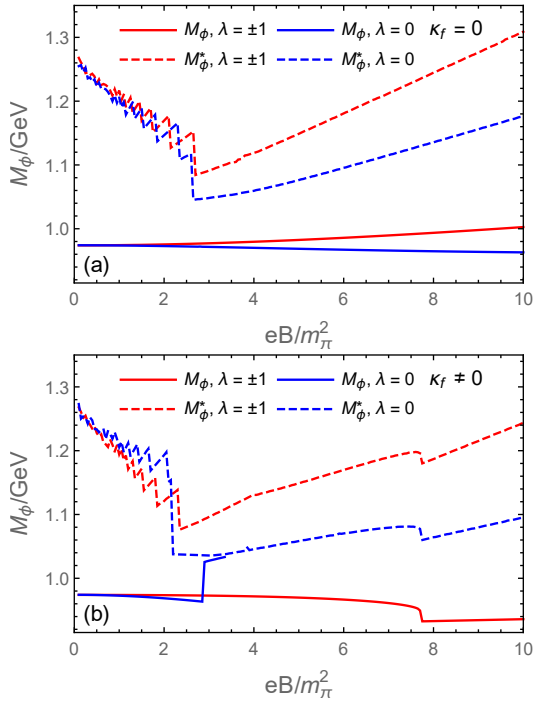


Figure 6. Dynamical masses as functions of eB for ϕ mesons at $T = 150$ MeV. Notations are the same as in Fig. 5.

ϕ meson masses. In absence of AMMs, the bound-state mass for $\lambda = 0$ decreases with an increasing eB , while that for $\lambda = \pm 1$ increases, as shown in Fig. 6 (a). Masses for resonance excitations oscillate when $eB < 2.5m_\pi^2$, and proportional to eB when $2.5m_\pi^2 < eB < 10m_\pi^2$. On the other hand, Fig. 6 (b) gives the ϕ meson masses when quark AMMs are nonzero. When $eB < 2.9m_\pi^2$, masses for bound states decrease in larger magnetic fields. The bound state with $\lambda = 0$ suddenly increases approach the mass of the resonance state at $eB \sim 2.9m_\pi^2$ and then dissociate when $eB \gtrsim 3.4m_\pi^2$, corresponding to the Mott transition. The masses for resonance excitations are nearly independent to the AMMs.

D. Spin alignment for ϕ mesons

Substituting the spectral functions calculated in subsection IVC into Eqs. (20) and (22), we derive the ϕ meson's spin alignment. Note that the bound states and resonance excitations are at different mass regions: the bound states have masses ~ 1 GeV or smaller, while masses for the resonance excitations have larger masses. Therefore we treat them as different kinds of particles and calculate their spin alignments separately.

In Fig. 7, we plot spin alignments ρ_{00} as functions of the temperature at $eB = 5m_\pi^2$. Spin alignments for bound states and resonance excitations are denoted as red solid lines and blue dashed lines, respectively. As a comparison, we also plot the result from a non-relativistic coalescence model [37],

$$\rho_{00}^{\text{Non-rel. coal.}} = \frac{1}{3} + \frac{4}{9T^2} \mu_s^2 B^2, \quad (34)$$

where $\mu_s = (1 + 2M_s \kappa_s) q_s / (2M_s)$ is the magnetic moment for the s quark, with $q_s = -1/3$. We first look at the case with AMMs $\kappa_f = 0$, given by Fig. 7 (a). The spin alignment ρ_{00} for bound states is significantly smaller than the result from the non-relativistic coalescence model when $T < 100$ MeV. The ρ_{00} for bound states decreases towards $1/3$ with an increasing T . For the temperature $T = 150$ MeV, ρ_{00} for bound states is in very good agreement with the coalescence model. Above 150 MeV, ρ_{00} for bound states is larger than the result from the coalescence model. Especially, bound states with $\lambda = \pm 1$ vanish when $T > 215$ MeV, leading to the result of $\rho_{00} = 1$ in this temperature region. On the other hand, the spin alignment ρ_{00} for resonance states is always larger than the result from the coalescence model except at very low temperatures. If we include nonvanishing AMMs, as shown in Fig. 7 (b), the spin alignment for bound states is always equal to zero because all bound states have $\lambda = \pm 1$, as indicated by Fig. 5 (b). The resonance states still have $\rho_{00} > \rho_{00}^{\text{Non-rel. coal.}} > 1/3$, which is similar to the case with $\kappa_f = 0$.

In Fig. 8 we show spin alignments as functions of the magnetic field strength. We focus on a fixed temperature $T = 150$ MeV and observe that ρ_{00} is proportional to eB

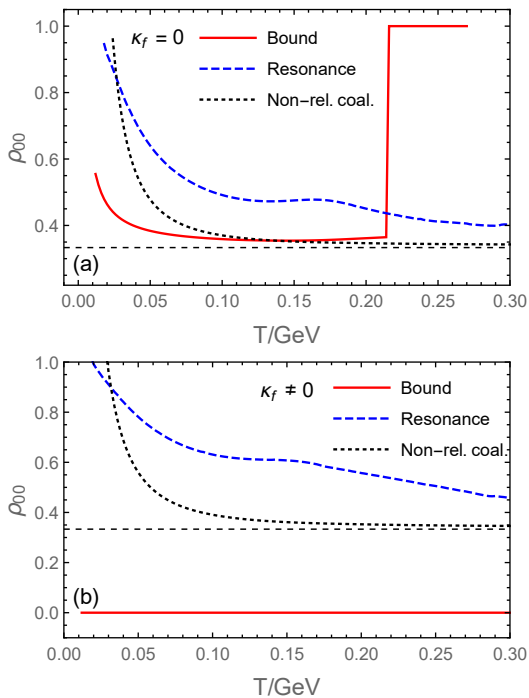


Figure 7. Spin alignments as functions of the temperature. The magnetic field strength is taken as $eB = 5m_\pi^2$. We take the quark AMMs $\kappa_f = 0$ in panel (a) and $\kappa_f \neq 0$ in panel (b). Red solid lines are spin alignment for bound states, calculated using the delta-function part in the spectral function 33, while blue dashed lines are spin alignment for resonance excitations, calculated using the continuum part in 33. Black dash-dotted lines are results from the non-relativistic coalescence model, given in Eq. (34).

when $\kappa_f = 0$, as shown in Fig. 8 (a). In the weak-field limit $eB \rightarrow 0$, ρ_{00} agrees with $1/3$, as expected. We find that the spin alignment for bound states agrees with the result of the non-relativistic coalescence model, while the spin alignment for resonance excitations is significantly larger. On the other hand, if we consider the AMMs, c.f., Fig. 8 (b), the ρ_{00} for bound states still agrees with the non-relativistic result when $eB < 2.5m_\pi^2$. It jumps to a negative value at $eB \sim 2.9m_\pi^2$, which is a straightforward result of the Mott transition for states with $\lambda = 0$. When the magnetic field strength is larger than $3.4m_\pi^2$, the bound state with $\lambda = 0$ dissociates in the thermal medium, resulting in a vanishing spin alignment $\rho_{00} = 0$. Meanwhile, the ρ_{00} for resonance excitations shows a non-monotonic structure: $\rho_{00} < 1/3$ when $eB < 2.6m_\pi^2$ and $\rho_{00} > 1/3$ when $eB > 2.6m_\pi^2$.

V. SUMMARY

In this manuscript, we study the mass splitting and the spin alignment for the vector ϕ meson in a hot magnetized matter. The three-flavor NJL model is used to properly include the chiral phase transition. In this

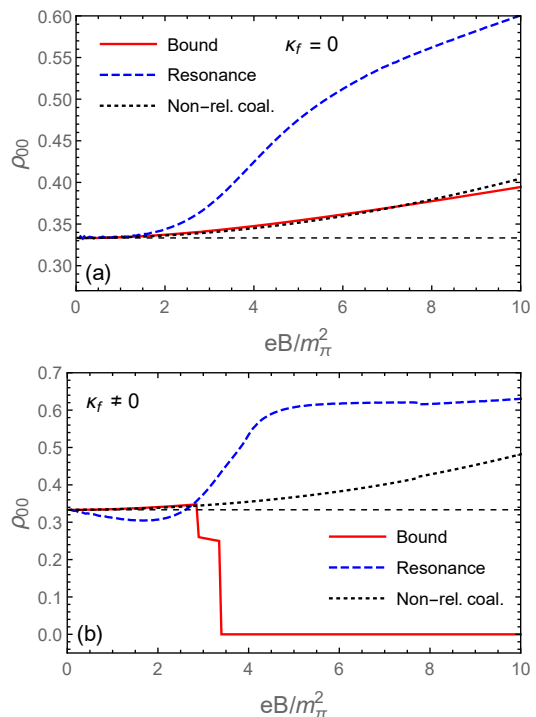


Figure 8. Spin alignments as functions of the magnetic field strength at temperature $T = 150$ MeV. Notations are the same as in Fig. 7.

framework, mesons are described as quantum fluctuations beyond the mean-field background. The meson's propagator is given by resumming quark bubbles at the random phase approximation. For a vector meson, the propagator is a Lorentz tensor perpendicular to the meson's momentum, which can be further projected into the spin space. The spin density matrix is then derived by the convolution of the spectral function and the Bose-Einstein distribution, while the spectral function is given by the imaginary part of the propagator. In this way, we are able to calculate the vector meson's spin alignment at the one-loop level in a thermal medium.

If we choose the spin quantization direction for the vector meson as the direction of the external magnetic field, the density matrix is then diagonal and spin states $\lambda = \pm 1$ are degenerate. We numerically calculated the spectral functions for ϕ mesons. In general the spectra can be separated into a delta-function part corresponding to a quark-antiquark bound state, and a continuum part corresponding to resonance excitations. We observe multi-peak structures in the continuum part, which is the result of Landau quantization for constituent quarks. The magnetic field leads to a mass splitting between states with $\lambda = 0$ and $\lambda = \pm 1$, resulting in the spin alignment $\rho_{00} \neq 1/3$ for the ϕ meson in a hot medium. If we only focus on the bound states, we find that $\rho_{00} > 1/3$ and is in good agreement with the result from the non-relativistic coalescence model. However, the spin alignment for resonance states gives a much larger result.

Since constitute quarks and free quarks have different magnetic moments, we incorporate the quark AMMs according to the constitute quark magnetic moments observed in experiments. The light-flavor quarks then show the inverse magnetic catalysis behaviors, and the chiral phase transition is first order. The AMMs then significantly modify the mass spectra and the spin alignment for the ϕ meson. We now observe a Mott transition for states with $\lambda = 0$ at $eB = 3.4 m_\pi^2$ and $T = 150$ MeV. Therefore in a magnetic field with $eB = 5 m_\pi^2$, all bound states have $\lambda = \pm 1$ and the spin alignment $\rho_{00} = 0$. On the other hand, in a weaker magnetic field, ρ_{00} still agree with the prediction from the non-relativistic coalescence model. We also notice that the spin alignment for resonance states show a non-monotonic structure: $\rho_{00} < 1/3$ when $eB < 2.6 m_\pi^2$ and $\rho_{00} > 1/3$ when $eB > 2.6 m_\pi^2$. We note that the constant AMMs significantly modify results of ρ_{00} , especially in stronger magnetic fields or at higher temperatures. Considering a different choice of AMMs, like in Ref. [86], may result in a different ρ_{00} , which is waiting for further studies.

Even though the spin quantization direction is fixed to the direction of the magnetic field in our numerical cal-

culations, we can easily generalize the results to the case that ρ_{00} is measured along any other direction, c.f., Eq. (27). This is achieved by performing a rotation in spin space for the density matrix. Therefore results in this work can be applied to study the ϕ meson's spin alignment in a fluctuating magnetic field. When the fluctuation is anisotropic in space, the spin alignment ρ_{00} will deviate from $1/3$. Therefore this work may help us better understand the role of the magnetic field in the ϕ mesons' spin alignment.

ACKNOWLEDGMENTS

The authors thank Prof. Mei Huang for enlightening discussions. X.L.S. is supported by the National Natural Science Foundation of China (NSFC) under grant No. 12047528, and by the Project funded by China Postdoctoral Science Foundation under grant No. 2021M701369. S.Y.Y, Y.L.Z., and D.F.H. are supported by the National Natural Science Foundation of China (NSFC) under grant Nos. 11735007, 11890711, and 11890710.

-
- [1] J. Rafelski and B. Muller, Phys. Rev. Lett. **36**, 517 (1976).
 - [2] D. E. Kharzeev, L. D. McLerran, and H. J. Warringa, Nucl. Phys. A **803**, 227 (2008), 0711.0950.
 - [3] V. Skokov, A. Y. Illarionov, and V. Toneev, Int. J. Mod. Phys. A **24**, 5925 (2009), 0907.1396.
 - [4] D. Kharzeev, K. Landsteiner, A. Schmitt, and H.-U. Yee, eds., *Strongly Interacting Matter in Magnetic Fields*, vol. 871 (2013), ISBN 978-3-642-37304-6, 978-3-642-37305-3.
 - [5] W.-T. Deng and X.-G. Huang, Phys. Rev. C **85**, 044907 (2012), 1201.5108.
 - [6] K. Tuchin, Phys. Rev. C **88**, 024911 (2013), 1305.5806.
 - [7] L. McLerran and V. Skokov, Nucl. Phys. A **929**, 184 (2014), 1305.0774.
 - [8] U. Gürsoy, D. Kharzeev, and K. Rajagopal, Phys. Rev. C **89**, 054905 (2014), 1401.3805.
 - [9] K. Tuchin, Phys. Rev. C **91**, 064902 (2015), 1411.1363.
 - [10] H. Li, X.-l. Sheng, and Q. Wang, Phys. Rev. C **94**, 044903 (2016), 1602.02223.
 - [11] Y. Chen, X.-L. Sheng, and G.-L. Ma, Nucl. Phys. A **1011**, 122199 (2021), 2101.09845.
 - [12] L. Yan and X.-G. Huang (2021), 2104.00831.
 - [13] Z. Wang, J. Zhao, C. Greiner, Z. Xu, and P. Zhuang, Phys. Rev. C **105**, L041901 (2022), 2110.14302.
 - [14] K. Fukushima, D. E. Kharzeev, and H. J. Warringa, Phys. Rev. D **78**, 074033 (2008), 0808.3382.
 - [15] D. T. Son and P. Surowka, Phys. Rev. Lett. **103**, 191601 (2009), 0906.5044.
 - [16] Z.-T. Liang and X.-N. Wang, Phys. Rev. Lett. **94**, 102301 (2005), [Erratum: Phys.Rev.Lett. 96, 039901 (2006)], nucl-th/0410079.
 - [17] F. Becattini, I. Karpenko, M. Lisa, I. Upsal, and S. Voloshin, Phys. Rev. C **95**, 054902 (2017), 1610.02506.
 - [18] L. Adamczyk et al. (STAR), Nature **548**, 62 (2017), 1701.06657.
 - [19] S. K. Das, S. Plumari, S. Chatterjee, J. Alam, F. Scardina, and V. Greco, Phys. Lett. B **768**, 260 (2017), 1608.02231.
 - [20] U. Gürsoy, D. Kharzeev, E. Marcus, K. Rajagopal, and C. Shen, Phys. Rev. C **98**, 055201 (2018), 1806.05288.
 - [21] A. Dubla, U. Gürsoy, and R. Snellings, Mod. Phys. Lett. A **35**, 2050324 (2020), 2009.09727.
 - [22] J.-J. Zhang, X.-L. Sheng, S. Pu, J.-N. Chen, G.-L. Peng, J.-G. Wang, and Q. Wang (2022), 2201.06171.
 - [23] A. Bzdak and V. Skokov, Phys. Lett. B **710**, 171 (2012), 1111.1949.
 - [24] I. Siddique, X.-L. Sheng, and Q. Wang, Phys. Rev. C **104**, 034907 (2021), 2106.00478.
 - [25] K. G. Klimenko, Z. Phys. C **54**, 323 (1992).
 - [26] V. P. Gusynin, V. A. Miransky, and I. A. Shovkovy, Phys. Rev. Lett. **73**, 3499 (1994), [Erratum: Phys.Rev.Lett. 76, 1005 (1996)], hep-ph/9405262.
 - [27] V. P. Gusynin, V. A. Miransky, and I. A. Shovkovy, Nucl. Phys. B **462**, 249 (1996), hep-ph/9509320.
 - [28] V. A. Miransky and I. A. Shovkovy, Phys. Rev. D **66**, 045006 (2002), hep-ph/0205348.
 - [29] G. Endrodi, M. Giordano, S. D. Katz, T. G. Kovács, and F. Pittler, JHEP **07**, 007 (2019), 1904.10296.
 - [30] G. S. Bali, F. Bruckmann, G. Endrodi, Z. Fodor, S. D. Katz, S. Krieg, A. Schafer, and K. K. Szabo, JHEP **02**, 044 (2012), 1111.4956.
 - [31] E. S. Fraga and A. J. Mizher, Nucl. Phys. A **820**, 103C (2009), 0810.3693.
 - [32] A. J. Mizher, M. N. Chernodub, and E. S. Fraga, Phys. Rev. D **82**, 105016 (2010), 1004.2712.
 - [33] J. O. Andersen, W. R. Naylor, and A. Tranberg, Rev. Mod. Phys. **88**, 025001 (2016), 1411.7176.
 - [34] M. Abdallah et al. (STAR) (2022), 2204.02302.

- [35] Z.-T. Liang and X.-N. Wang, Phys. Lett. B **629**, 20 (2005), nucl-th/0411101.
- [36] A. H. Tang, B. Tu, and C. S. Zhou, Phys. Rev. C **98**, 044907 (2018), 1803.05777.
- [37] Y.-G. Yang, R.-H. Fang, Q. Wang, and X.-N. Wang, Phys. Rev. C **97**, 034917 (2018), 1711.06008.
- [38] X.-L. Xia, H. Li, X.-G. Huang, and H. Zhong Huang, Phys. Lett. B **817**, 136325 (2021), 2010.01474.
- [39] J.-H. Gao, Phys. Rev. D **104**, 076016 (2021), 2105.08293.
- [40] B. Müller and D.-L. Yang, Phys. Rev. D **105**, L011901 (2022), 2110.15630.
- [41] F. Li and S. Y. F. Liu (2022), 2206.11890.
- [42] D. Wagner, N. Weickgenannt, and E. Speranza (2022), 2207.01111.
- [43] X.-L. Sheng, L. Oliva, and Q. Wang, Phys. Rev. D **101**, 096005 (2020), [Erratum: Phys.Rev.D 105, 099903 (2022)], 1910.13684.
- [44] X.-L. Sheng, Q. Wang, and X.-N. Wang, Phys. Rev. D **102**, 056013 (2020), 2007.05106.
- [45] X.-L. Sheng, L. Oliva, Z.-T. Liang, Q. Wang, and X.-N. Wang (2022), 2206.05868.
- [46] X.-L. Sheng, L. Oliva, Z.-T. Liang, Q. Wang, and X.-N. Wang (2022), 2205.15689.
- [47] Y. Nambu and G. Jona-Lasinio, Phys. Rev. **124**, 246 (1961).
- [48] Y. Nambu and G. Jona-Lasinio, Phys. Rev. **122**, 345 (1961).
- [49] S. Klimt, M. F. M. Lutz, U. Vogl, and W. Weise, Nucl. Phys. A **516**, 429 (1990).
- [50] U. Vogl, M. F. M. Lutz, S. Klimt, and W. Weise, Nucl. Phys. A **516**, 469 (1990).
- [51] S. P. Klevansky, Rev. Mod. Phys. **64**, 649 (1992).
- [52] M. Buballa, Phys. Rept. **407**, 205 (2005), hep-ph/0402234.
- [53] M. K. Volkov and A. E. Radzhabov, Phys. Usp. **49**, 551 (2006), hep-ph/0508263.
- [54] K. Fukushima, Phys. Rev. D **77**, 114028 (2008), [Erratum: Phys.Rev.D 78, 039902 (2008)], 0803.3318.
- [55] T. Hatsuda and T. Kunihiro, Phys. Rept. **247**, 221 (1994), hep-ph/9401310.
- [56] H. Liu, L. Yu, and M. Huang, Phys. Rev. D **91**, 014017 (2015), 1408.1318.
- [57] S. S. Avancini, W. R. Tavares, and M. B. Pinto, Phys. Rev. D **93**, 014010 (2016), 1511.06261.
- [58] S. S. Avancini, R. L. S. Farias, M. Benghi Pinto, W. R. Tavares, and V. S. Timóteo, Phys. Lett. B **767**, 247 (2017), 1606.05754.
- [59] S. Mao, Phys. Rev. D **99**, 056005 (2019), 1808.10242.
- [60] M. Coppola, D. Gómez Dumm, and N. N. Scoccola, Phys. Lett. B **782**, 155 (2018), 1802.08041.
- [61] N. Chaudhuri, S. Ghosh, S. Sarkar, and P. Roy, Phys. Rev. D **99**, 116025 (2019), 1907.03990.
- [62] K. Xu, J. Chao, and M. Huang, Phys. Rev. D **103**, 076015 (2021), 2007.13122.
- [63] M. Wei, Y. Jiang, and M. Huang (2020), 2011.10987.
- [64] S. Yang, M. Jin, and D. Hou, Chin. Phys. C **46**, 043107 (2022), 2108.12207.
- [65] V. A. Miransky and I. A. Shovkovy, Phys. Rept. **576**, 1 (2015), 1503.00732.
- [66] G. Cao, Eur. Phys. J. A **57**, 264 (2021), 2103.00456.
- [67] L. Brekke and J. L. Rosner, Comments Nucl. Part. Phys. **18**, 83 (1988).
- [68] L. Chang, Y.-X. Liu, and C. D. Roberts, Phys. Rev. Lett. **106**, 072001 (2011), 1009.3458.
- [69] S. Fayazbakhsh and N. Sadooghi, Phys. Rev. D **90**, 105030 (2014), 1408.5457.
- [70] A. Ayala, C. A. Dominguez, L. A. Hernandez, M. Loewe, and R. Zamora, Phys. Lett. B **759**, 99 (2016), 1510.09134.
- [71] G. 't Hooft, Phys. Rev. Lett. **37**, 8 (1976).
- [72] V. I. Ritus, Annals Phys. **69**, 555 (1972).
- [73] V. I. Ritus, Sov. Phys. JETP **48**, 788 (1978).
- [74] J. I. Kapusta and C. Gale, *Finite-temperature field theory: Principles and applications*, Cambridge Monographs on Mathematical Physics (Cambridge University Press, 2011), ISBN 978-0-521-17322-3, 978-0-521-82082-0, 978-0-511-22280-1.
- [75] W. Pauli and F. Villars, Rev. Mod. Phys. **21**, 434 (1949).
- [76] S. Carignano and M. Buballa, Phys. Rev. D **101**, 014026 (2020), 1910.03604.
- [77] Y. Dothan, Physica A **114**, 216 (1982).
- [78] N. F. MOTT, Rev. Mod. Phys. **40**, 677 (1968).
- [79] J. Hufner, S. P. Klevansky, and P. Rehberg, Nucl. Phys. A **606**, 260 (1996).
- [80] P. Costa, M. C. Ruivo, and Y. L. Kalinovsky, Phys. Lett. B **560**, 171 (2003), hep-ph/0211203.
- [81] D. Blaschke, A. Dubinin, A. Radzhabov, and A. Wergieluk, Phys. Rev. D **96**, 094008 (2017), 1608.05383.
- [82] S. Mao, Chin. Phys. C **45**, 021004 (2021), 1908.02851.
- [83] T. Ishikawa et al., Phys. Lett. B **608**, 215 (2005), nucl-ex/0411016.
- [84] R. Muto et al. (KEK-PS-E325), Phys. Rev. Lett. **98**, 042501 (2007), nucl-ex/0511019.
- [85] X. Qian et al. (CLAS), Phys. Lett. B **680**, 417 (2009), 0907.2668.
- [86] M. Kawaguchi and M. Huang (2022), 2205.08169.

Appendix A: Quark propagator

In the presence of the the anomalous magnetic moment, the fermion propagator in momentum space is given by [65],

$$S_f(p) = ie^{-p_\perp^2/|q_f B|} \sum_{n=0}^{\infty} (-1)^n D_n^f(p) \frac{1}{\mathcal{M}(p) - 2n|q_f B|}, \quad (\text{A1})$$

where f labels the flavor of quark, and $\mathbf{p}_\perp \equiv (p_x, p_y)$ with $p_\perp \equiv \sqrt{p_x^2 + p_y^2}$ being the transverse momentum. The numerator of the n -th Landau level contribution is

$$D_n^f(p) = 2 \left(p^0 \gamma^0 - p_z \gamma^3 + \tilde{\Sigma} \right) \left[\mathcal{P}_+ L_n \left(\frac{2p_\perp^2}{|q_f B|} \right) - \mathcal{P}_- L_{n-1} \left(\frac{2p_\perp^2}{|q_f B|} \right) \right] + 4\mathbf{p}_\perp \cdot \boldsymbol{\gamma}_\perp L_{n-1}^1 \left(\frac{2p_\perp^2}{|q_f B|} \right), \quad (\text{A2})$$

where the projection operators $\mathcal{P}_\pm \equiv [1 \pm i\gamma^1 \gamma^2 \text{sign}(q_f B)]/2$, $L_n^i(x)$ is the generalized Laguerre polynomial with $L_n(x) \equiv L_n^0(x)$, and the modified self-energy is given by

$$\tilde{\Sigma} = M_f + i\kappa_f q_f B \gamma^1 \gamma^2. \quad (\text{A3})$$

The explicit form of the matrix \mathcal{M} is given in Ref. [65], from which we derive

$$\frac{1}{\mathcal{M}(p) - 2n|q_f B|} = \frac{1}{U_n} [(p^0)^2 - (p_z)^2 - M_f^2 - 2n|q_f B| + (\kappa_f q_f B)^2 + 2\kappa_f q_f B(p_z \gamma^0 \gamma^5 - p^0 \gamma^3 \gamma^5)] , \quad (\text{A4})$$

where the common denominator U_n is given by

$$U_n = [(p^0)^2 - (p_z)^2 - M_f^2 - 2n|q_f B| - (\kappa_f q_f B)^2]^2 - 4(M_f^2 + 2n|q_f B|)(\kappa_f q_f B)^2 . \quad (\text{A5})$$

Note that the eigenenergies in Eq. (6) can be determined by the locations of the poles of the propagator. For Landau levels $n > 0$, this can be achieved by solving $U_n = 0$.